Available online at www.sciencedirect.com
SCIENCE DIRECT®
PERGAMON
Electrochimica Acta 48 (2003) 1551–1557
ELECTROCHIMICA Acta
www.elsevier.com/locate/electacta

Conductivity of CGO and CSO ceramics obtained from freeze-dried precursors

D. Pérez-Coll [a], P. Núñez [a], J.R. Frade [b,*], J.C.C. Abrantes [c]

[a] Departamento de Química Inorgánica, Universidad de La Laguna, E-38200 La Laguna, Tenerife, Spain
[b] Departamento de Engenharia Cerâmica e do Vidrio, CICELO Universidade de Aveiro, 3810°-193 Aveiro, Portugal
[c] ESTG, Instituto Politécnico de Viana do Castelo, 4900 Viana do Castello, Portugal

Received 21 October 2002; received in revised form 6 January 2003

Abstract

$Ce_{0.8}Gd_{0.2}O_{1.9}$ (CGO) and $Ce_{0.8}Sm_{0.2}O_{1.9}$ (CSO) have been prepared as polycrystalline materials using a freeze-dried precursor. This method yields amorphous nanometric powders. Crystallization of the fluorite phase occurred on heating at 600 °C or higher temperatures. The grain size of freeze-dried powders increases to about 100 nm after calcination at 800 °C, or about 200 nm after firing at 1000 °C. Freeze-dried powders were used to prepare dense ceramic disks by sintering at 1400 °C. Some disks were sintered at 1000 °C by adding small amounts of cobalt nitrate solution to assist the densification. The electrical conductivity results obtained for these gadolinia-doped ceria and samaria-doped ceria ceramics are similar to those obtained for CGO pellets obtained from commercial nanopowders (Rhodia). Though the bulk conductivity of CSO is probably higher than that of CGO, its grain boundary conductivity is inferior, and tends to control the overall behaviour, at least at relatively low temperatures.

Keywords: Ceria electrolytes; Freeze drying; Electrical conductivity; Grain boundaries

1. Introduction

Solid electrolytes exhibiting high oxygen ion conductivity are of special interest for their application in high-temperature system such as solid oxide fuel cells (SOFCs), oxygen sensors, electrochemical oxygen pumps, systems for partial oxidation of methane or other hydrocarbons, etc. SOFCs are promising energy conversion systems with a great potential for high efficiency and low pollution [1,2]. The state of the art electrolyte material yttria-stabilized zirconia (YSZ) is expected to operate at 800–1000 °C. However, reducing the operating temperature allows the use of cheaper construction materials and more reliable seals. New materials are thus investigated to lower the operating temperature to 500–700 °C, which includes new electrolyte materials [3] with higher ionic conductivity.

Gadolinia (CGO) or samaria-doped ceria (CSO) are attractive as electrolytes for intermediate-temperature solid oxide fuel cells (IT-SOFCs) [4,5] and as alternative anode materials for direct methane conversion to avoid carbon deposition in Ni/YSZ anodes [6,7]. Ce^{4+} reduces to Ce^{3+} at elevated temperature and reducing atmospheres resulting in higher oxygen deficiency, n-type conductivity, and phase changes for excessive deficiency. Additions of CeO_2 with Ln_2O_3 (Ln = Y, Gd, Sm, etc.) increase the chemical stability, increase the ionic conductivity, and suppress the reducibility of ceria-based materials. The most effective additives are Gd_2O_3 and Sm_2O_3 possibly because they minimize the changes in lattice parameters [8]; this was confirmed by atomistic computer simulations [9] based on the binding energy between trivalent cations and oxygen vacancies, and the corresponding lattice relaxation energy. These simulations suggest that the optimum radius for the trivalent cation in the ceria-based oxide nearly corresponds to the radius of Gd^{3+}, thus supporting the common finding that ceria–gadolinia (CGO) should possess the highest

* Corresponding author.
E-mail addresses: nunez@ull.es (P. Núñez), jfrade@cv.ua.pt (J.R. Frade).

0013-4686/03/$ - see front matter © 2003 Elsevier Science Ltd. All rights reserved.
doi:10.1016/S0013-4686(03)00027-6

values of ionic conductivity [4]. Yet, other authors reported higher conductivity values for ceria–samaria (CSO) materials [10,11].

For operating temperatures in the order of 1000 °C, ceria-based electrolytes become partly reduced at the fuel side of a cell causing significant electronic conductivity and the resulting efficiency losses due to the internal short circuit current. Some literature data suggest somewhat larger ionic domain for CSO electrolytes than for CGO, as demonstrated by differences in voltage–current density results obtained with the corresponding fuel cells [10]. However, the changes of oxygen stoichiometry with oxygen partial pressure are similar for CSO and CGO [12], thus failing to demonstrate significant differences in reducibility. The onset of the n-type electronic conductivity has also been estimated from the dependence of conductivity on the oxygen partial pressure [10,13,14]. This method is not an exempt of errors, and this might explain some of the differences between results reported by different authors. Other authors thus resorted to alternative Hebb-Wagner ion blocking methods [15,16] to measure the electronic conductivity. Nevertheless, there is a consensus that the reducibility under fuel conditions and the electronic conductivity are suppressed with decreasing operating temperature. These materials have thus been proposed mainly for the range 500–700 °C [4].

It is thus far from clear whether the properties of CGO exceed those of CSO. Some of the differences between results reported by different authors might be due to factors such as methods of powder preparation and/or sintering schedule [17,18], probably due to resistive grain boundaries. Relatively high temperatures have been used to attain close to full density and larger grain sizes. Yet, ceramics with larger grain sizes often show poor mechanical stability. In addition, some results suggest that the grain boundary conductivity goes through a minimum on varying the average grain size [19]. Other authors thus proposed a method to obtain dense sub-micrometer ceramics at about 1000 °C by using sintering additives in the form of nitrate solutions (e.g. cobalt nitrate) [20].

This work thus re-examines the differences between the conductivities of CGO and CSO. The samples were carefully prepared under identical conditions for both compositions to minimize differences related to the preparation methods. A freeze-drying method was used to obtain homogeneous nanocrystalline precursors, as described below. Samples with sub-micrometric grain size were sintered at 1000 °C with a sintering aid, and higher temperatures were used to obtain samples with larger grain sizes. The corresponding grain boundary and bulk contributions could thus be distinguished by impedance spectroscopy.

2. Preparation of powders and ceramic samples

In this work, $Ce_{0.8}Gd_{0.2}O_{1.9}$ (CGO) and $Ce_{0.8}Sm_{0.2}O_{1.9}$ (CSO) were obtained from freeze-dried precursor powders. This preparative method yields powders with grain size in the nanoscale range. Ceramic samples were prepared from those precursor powders.

The required stoichiometric amounts of $Ce(NO_3)_3 \cdot 6H_2O$ (Aldrich, 99.9%) and $Gd(NO_3)_3 \cdot 6H_2O$ (Aldrich, 99.9%) were dissolved in distilled water and mixed. This solution was taken into a separating-funnel and was driven into liquid nitrogen by dropwise addition with continuous stirring. This flash cooling provides small ice crystals, which were dehydrated by sublimation in a freeze drier (Heto, Lyolab 3000) for 3 days. The precursors obtained in this way were ground in a mortar and calcined in air for 2 h at 600, 800, 1000, 1200 and 1400 °C. All materials were identified by XRD using a Phillips X'pert powder diffractometer with Cu Kα radiation and a graphite secondary monochromator. CSO powder was prepared in a similar way using $Ce(NO_3)_3 \cdot 6H_2O$ (Aldrich, 99.9%) and $Sm(NO_3)_3 \cdot 6H_2O$ (Aldrich, 99.9%) as starting materials. Crystalline and single-phase CGO and CSO powders were obtained by calcining the as-prepared freeze-dried powders at temperatures above 600 °C. Figs. 1 and 2 show the X-ray patterns of CGO and CSO powders obtained after calcining the precursor for 2 h at 600, 800, 1000, 1200 and 1400 °C. The as-prepared powders were amorphous. The crystallinity of the samples increases with increasing temperature from 600 to 1200 °C. Above

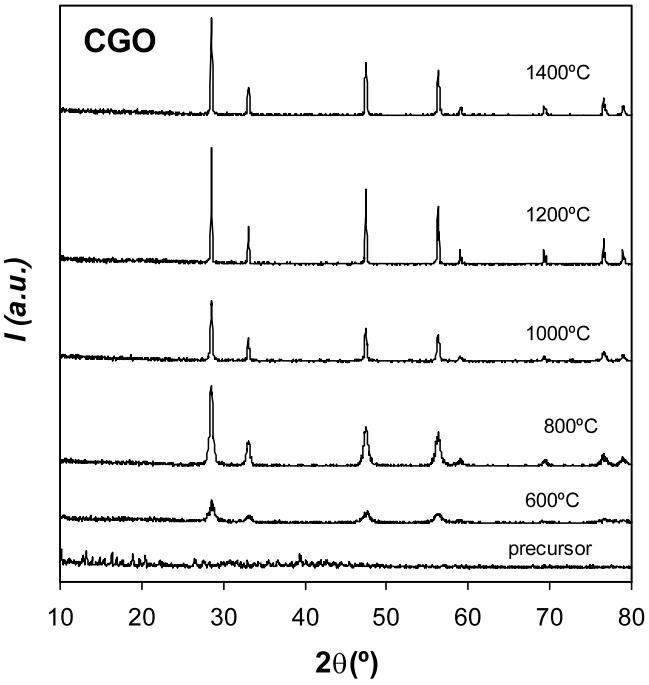

Fig. 1. X-ray patterns of CGO powders obtained by freeze-drying as prepared and calcined at 600, 800, 1000, 1200 and 1400 °C.

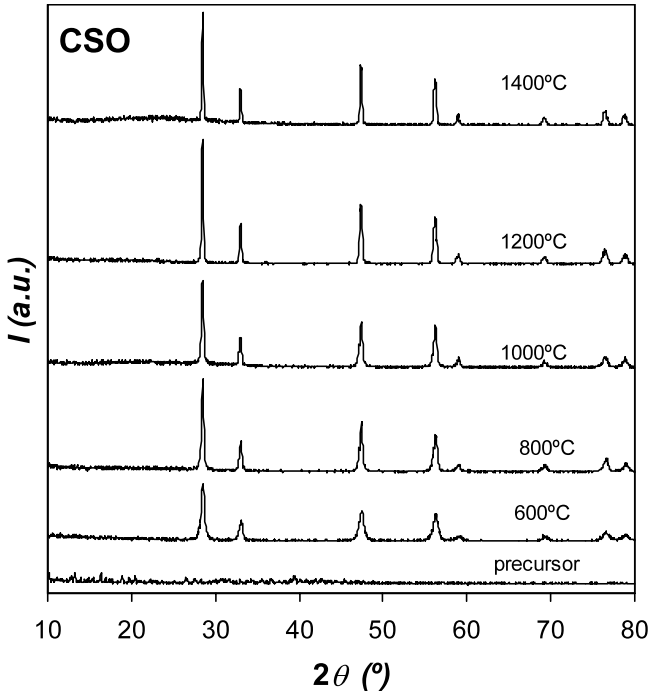

Fig. 2. X-ray patterns of CSO powders obtained by freeze-drying as prepared and calcined at 600, 800, 1000, 1200 and 1400 °C.

1200 °C, the X-ray pattern does not show noticeable changes.

Freeze-dried powders, pre-heated at 1200 °C for 2 h, were used for the preparation of ceramic CGO and CSO samples. Solutions of cobalt nitrate ($Co(NO_3)_2 \cdot 6H_2O$, Panreac) in ethanol were also used to impregnate the starting powders. The resulting pastes were ground in a mortar for about 20 min, dried and then calcined at 650 °C for 1 h.

Cylindrical pellets, 13 mm in diameter and about 2 mm in height, were obtained by uniaxial pressing at 1 t for 30 s, and then at 3 t for 1 min. Cobalt-doped pellets were sintered at 1000 °C for 5 h. Samples without cobalt were sintered at 1400 °C for 5 h. The density of each sintered pellet was measured by the Archimedes method with distilled water. The microstructures of the samples were studied by scanning electron microscopy (Jeol Ltd., Model JSM-6300). Scanning electron micrographs of the 2 cat% Co-doped CGO and undoped CGO before sintering are shown in Fig. 3. The average particle diameters of samples were determined from the photographs. CGO calcined at 800 °C along 2 h shows a grain size less than 100 nm.

Table 1
Sintering temperature, density and percentage of sintering of CGO, CGO+3 cat% Co, CGO+2 cat% Co and CSO

Sample	Temperature (°C)	Density (g/cm^3)	Relative density (%)
CGO	1400	6.80	93.9
CGO+3% Co	1000	6.86	94.7
CGO+2% Co	1000	6.76	93.4
CSO	1400	6.70	93.3

Table 1 summarizes the values of sintering temperatures, apparent density, and percentage of cubic phase retained at room temperature after sintering. As one can observe, the presence of small amounts of Co decreases the sintering temperature from 1400 to 1000 °C to give about 93–94% of the theoretical density. The results show that Co additions have a remarkable effect on sintering of CGO. The microstructure of CGO doped with 1 and 2 cat% Co, sintered at 1000 °C for 5 h is shown in Fig. 4.

3. Electrical measurements

AC impedance spectroscopy was performed on the sintered pellets using an FRA (Solartron, model 1260). Impedance measurements were made in air over the temperature range 200–700 °C and the frequency range $0.1–10^7$ Hz. Measurements at temperatures above would be likely to cause further coarsening of submicrometer ceramics. The excitation voltage was 15 mV for the range 400–700 °C and 100 mV for the range 200–400 °C. To ensure good contact between the platinum wires and the samples, each side of the pellets

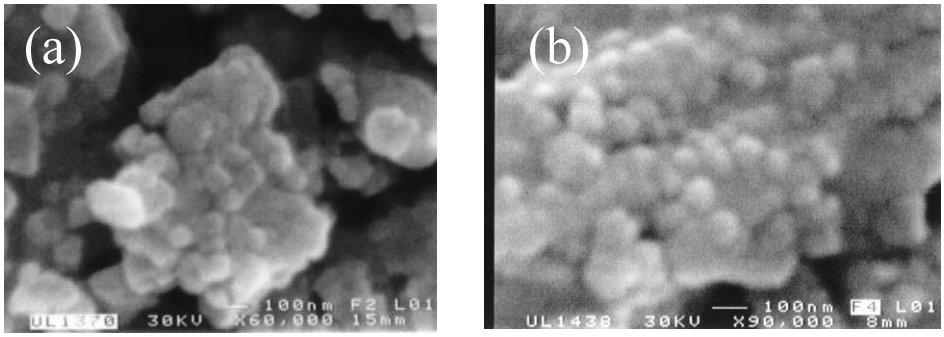

Fig. 3. Scanning electron micrographs of CGO powders with and without 2% Co addition and calcined at 800 °C for 2 h.

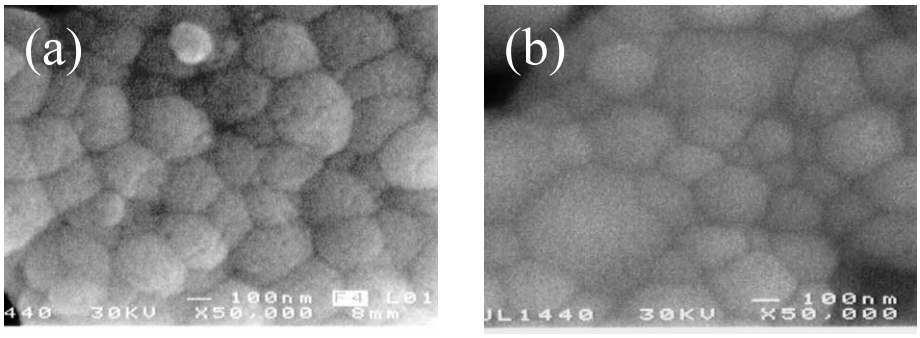

Fig. 4. Scanning electron micrographs of CGO samples sintered at 1000 °C with 1 and 2% Co sintering additives.

was painted in a diameter of 5.85 mm with platinum paste and baked at 900 °C for 12 h.

Typical impedance spectra (Fig. 5) reveal contributions which can be ascribed to the bulk, grain boundaries, and electrode processes based on differences in relaxation frequency and capacitance. The relaxation frequencies of the bulk and grain boundary contributions increase with temperature, thus preventing the detection of separate bulk and grain boundary arcs at temperatures above about 400 °C. In this case, one can obtains only the value of total resistance, and the corresponding conductivity, $\sigma = L/AR$, taking into account the thickness to area ratio L/A. The temperature dependence of total conductivity (Fig. 6) clearly shows significant deviations from the Arrhenius law:

$$\sigma = \left(\frac{\sigma_0}{T}\right)\exp\left(-\frac{E_a}{kT}\right), \quad (1)$$

thus indicating significant differences between low- and high-temperature conduction mechanisms. The most likely reasons for this change in activation energy are the increasing role of the grain boundary resistance and probably also the increasing interactions between the charge carriers (oxygen vacancies) and the trivalent additive (Gd^{3+} or Sm^{3+}) with decreasing temperature [21].

Fitting the spectra obtained at temperatures in the range 200–400 °C allowed one to separate the microstructural contributions ascribed to the bulk (grain interiors) and grain boundaries. The corresponding bulk conductivity results are shown in Fig. 7, and the grain boundary results are shown in Fig. 8, after accounting for the geometric ratio L/A of the sample.

The results shown in Figs. 7 and 8 may be extrapolated to higher temperatures to estimate the corresponding bulk and grain boundary conductivity values under prospective working conditions (above 500 °C). Otherwise, one should attempt to lower the grain boundary relaxation frequency range to be able to reveal this contribution at higher temperatures. However, this is a difficult task, which is unlikely to be reached by adjusting the average grain size, and/or the

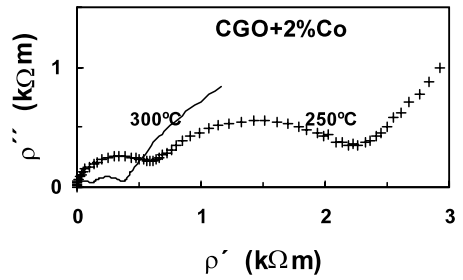

Fig. 5. Typical impedance spectra obtained at 250 and 300 °C for a CGO sample sintered at 1000 °C with 2% Co added.

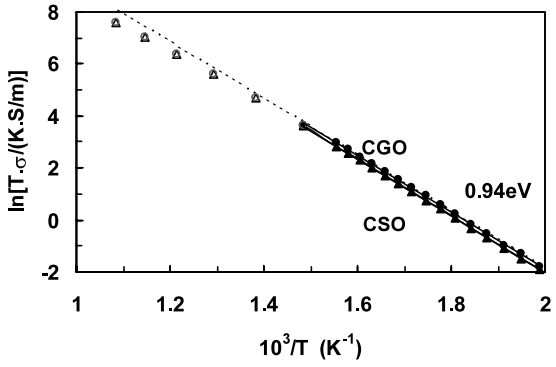

Fig. 6. Temperature dependence of total conductivity of CGO (●, ○) and CSO (▲, △) samples sintered at 1400 °C.

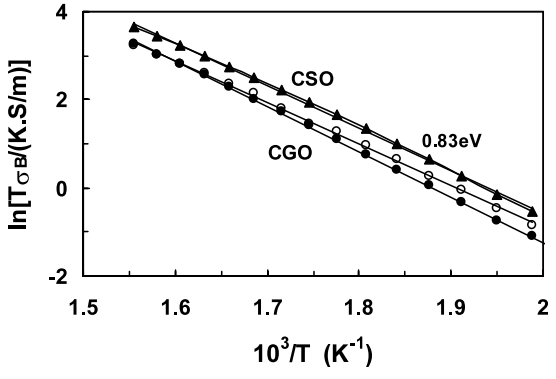

Fig. 7. Bulk conductivity obtained for CGO (●) and CSO (▲) sintered at 1400 °C without Co addition, and for CGO sintered at 1000 °C with 2% Co sintering additive (○).

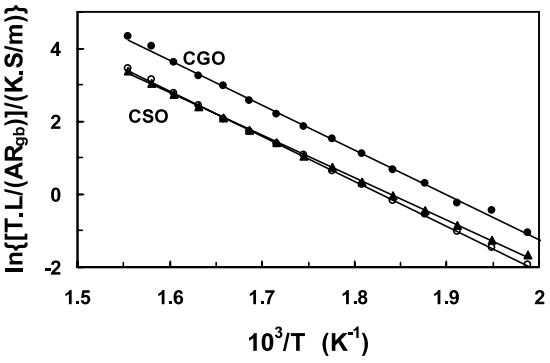

Fig. 8. Grain boundary resistance results after correcting for the thickness to area ratio (L/A) obtained for CGO (●) and CSO (▲) sintered at 1400 °C without Co addition, and for CGO sintered at 1000 °C with 2% Co sintering additive (○).

sample geometry (i.e. the thickness to area ratio). In fact, these changes exert opposite effects on the resistance and capacitance of the grain boundary contribution, and should not give rise to significant changes in the corresponding relaxation frequency $f_{gb} = (2\pi C_{gb}R_{gb})^{-1}$.

The temperature dependence of the bulk conductivity yielded the values of activation energy shown in Table 2. These values of activation energy are clearly above the values reported for conductivity data at high temperatures, but are closer to results reported for temperatures below a transition temperature in the range 500–600 °C [21,22]; this is consistent with the assumption that defect interactions contribute to the increase in activation energy with decreasing temperature shown in Fig. 6.

The grain boundary results (Fig. 8) show even higher values of activation energy thus, confirming that grain boundaries also play a major role on the increase in activation energy of total conductivity in the low-temperature range. The poorer results obtained for the CGO sample sintered at lower temperatures (with sintering additive) are easily related to smaller grain sizes. However, this does not explain the main differences between the results obtained for CSO and CGO samples fired at identical temperature (1400 °C), possibly because the nature of blocking grain boundaries might be dependent on compositional changes. In this study, these changes correspond to different trivalent additive and possibly also the presence of a sintering additive (2% Co) added to one of the CGO samples.

A comparison of the true grain boundary conductivity results is likely to indicate whether the nature of grain boundaries and their properties are significantly dependent on composition. Such estimates may rely on the expected applicability of the brick layer model, as found for other types of materials [23,24]. The proposed model accounts for changes in grain size, but may be ill suited to analyze the present data, because the nature of the grain boundary may have been altered. In addition, one may need additional information about the grain boundary thickness. Alternatively, one may take into account that the effective area to thickness ratio $(A/L)_{eff}$ plays opposite effects on the grain boundary capacitance and grain boundary resistance. These effects cancel in the peak relaxation frequency $f_{gb} = (2\pi C_{gb}R_{gb})^{-1} = \sigma_{gb}/2\pi\varepsilon_0\varepsilon_r$, and thus

$$\sigma_{gb} = 2\pi f_{gb}\varepsilon_0\varepsilon_r,$$

where $\varepsilon_0 = 8.854 \times 10^{-12}$ F is the permittivity of vacuum and the dielectric constant ε_r may be obtained from values of bulk capacitance or from literature data.

The dielectric constant of ceria-based materials is probably relatively small and some authors [5] reported values as low as $\varepsilon_r = 11$. However, one expects greater values from other sources. Ref. [18] presented impedance spectra for ceria–yttria samples from which one may extract estimates of dielectric constant of about 36 for single crystals and about 100 for ceramic samples. These estimates were obtained by taking into account the values of the bulk resistance, relaxation frequency, and area to thickness ratio. From another work reported by Christie and van Berkel [19], one estimated $\varepsilon_r = 30$. This shows that significant differences might be found from different sources, probably because the values of bulk capacity might be close to or even lower than the detection limits of the equipment used; this is often higher than 10 pF, and might be as high as 100 pF. The fitting parameters obtained from spectra acquired in this work include values of bulk capacity exceeding 10 pF. The corresponding values of dielectric constant ($\varepsilon_r > 100$) are probably crude results, because the correct value of bulk capacity is probably below the detection of the equipment.

In order to improve the correctness of the measurements of bulk capacity, one should use samples with large area to thickness ratio, to attain values of bulk

Table 2
Values of activation energy of the bulk and grain boundary conductivities of a CSO sample sintered at 1400 °C, and CGO samples sintered at 1400 °C without sintering additives, and sintered at 1000 °C with 2% Co addition

Sample	Sintering temperature (°C)	Bulk E_a (eV)	Grain boundary E_a (eV)
CSO	1400	0.89	0.93
CGO	1400	0.83	0.95
CGO+2% Co	1000	0.82	0.96

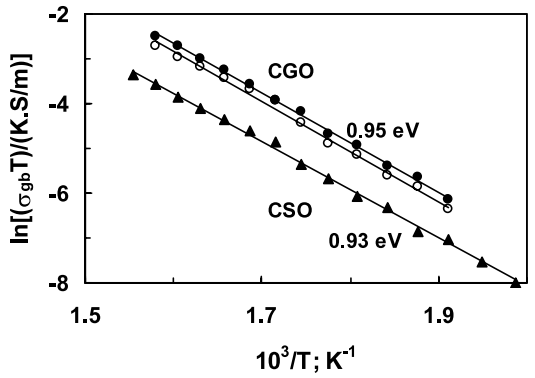

Fig. 9. Estimates of the true grain boundary conductivity obtained for CGO (●) and CSO (▲) sintered at 1400 °C without Co addition, and for CGO sintered at 1000 °C with 2% Co sintering additive (○). A typical value of dielectric constant $\varepsilon_r = 30$ was assumed.

capacity well within the range of the equipment. Thus, one assumes a typical value ($\varepsilon_r = 30$) extracted from the work of Christie and van Berkel, which was based on samples with relatively large area to thickness ratio (A/L close to 1 m). The results shown in Fig. 9 were computed for $\varepsilon_r = 30$. These values should at least give the correct order of magnitude of the true grain boundary conductivity and can be used to analyze the differences between CGO and CSO. One thus concludes from Fig. 9 that the performance of CSO ceramics is more likely to be affected by resistive grain boundaries, even for similar microstructures. The low conductivity of the grain boundaries in CSO ceramics may also explain some different views expressed by different authors concerning the ceria-based systems with highest conductivity.

The results in Fig. 9 also show that the grain boundary conductivity is only weakly affected by the sintering additive (2% Co). One thus concludes that the main differences between CGO samples with and without sintering additive (Fig. 8) are related to differences in grain size, rather than true differences in grain boundary nature.

Further work is certainly needed to confirm the present findings, and one is thus extending this work; this requires the preparation and characterization of additional samples with different thickness to area ratio and additional microstructural changes which might be distinguished by impedance spectroscopy. One expects to confirm the differences between CSO and CGO ceramics. Detailed TEM work of grain boundaries will be performed to attain a better understanding of the grain boundaries in these materials, including the effects of Co additions used to assist the low-temperature sintering and preparation of ceramic samples with submicrometer grain sizes.

4. Conclusions

A freeze-drying method is suitable to prepare nanometric powders of ceria-based materials. The as-prepared powders are amorphous but the fluorite phase is readily formed by heating at 600 °C or higher temperatures. These powders were used to prepare ceramic samples of ceria–gadolinia and ceria–samaria. Relatively high temperatures are needed to densify. Submicrometric samples were prepared by firing at lower temperatures with cobalt nitrate as a sintering additive. Both types of ceramic samples show the overall electrical behaviour includes contributions ascribed to the bulk (grain interiors) and grain boundaries, at least at temperatures below about 500 °C. Though the bulk conductivity of CSO is higher than for CGO, the CGO ceramics are less affected by the resistive grain boundaries and show higher overall conductivity for samples with similar grain sizes. The bulk conductivity shows significantly higher activation energy in the low-temperature range than for higher temperatures, probably due to interaction of the charge carriers (oxygen vacancies) with the trivalent additive (Gd^{3+} or Sm^{3+}).

Acknowledgements

The authors acknowledge the financial support by the research program CICYT-FEDER-1FD97-1422-MAT and MCyT-MAT-2001-3334, and the Portuguese Foundation for Science and Technology (FCT-POCT/CTM/39381/2001). Travel grants were provided by the European Science Foundation (OSSEP Programme) for bilateral cooperation between the Spanish and Portuguese institutions. One of the authors (D.P.C.) thanks Convenio Cajacanarias-Universidade de La Laguna for a grant.

References

[1] N.Q. Minh, T. Takahashi, Science and Technology of Ceramic Fuel Cells, Elsevier, Amsterdam, 1995.
[2] P.J. Gellings, H.J.M. Bouwmeester, The CRC Handbook of Solid State Ionics Electrochemistry, CRC Press, Boca Raton, FL, 1997.
[3] H.L. Tuller, Solid State Ionics 131 (2000) 143.
[4] B.C.H. Steele, Solid State Ionics 129 (2000) 95.
[5] M. Mogensen, N.M. Sammes, G.A. Tompsett, Solid State Ionics 129 (2000) 63.
[6] O.A. Marina, C. Bagger, S. Primdahl, M. Mogensen, Solid State Ionics 123 (1999) 199.
[7] E.S. Putna, J. Stubenrauch, J.M. Vohs, R.J. Gorte, Langmuir 11 (1995) 4832.
[8] D.-J. Kim, J. Am. Ceram. Soc. 72 (1989) 1415.
[9] L. Minervini, M.O. Zacate, R.W. Grimes, Solid State Ionics 116 (1999) 339.
[10] H. Yahiro, K. Eguchi, H. Arai, Solid State Ionics 36 (1989) 71.
[11] H. Inaba, H. Tagawa, Solid State Ionics 83 (1996) 1.

[12] D. Schneider, M. Godickemeier, L.J. Gauckler, J. Electroceram. 1 (1997) 165–172.
[13] H. Yahiro, K. Eguchi, H. Arai, Solid State Ionics 21 (1986) 37.
[14] M. Mogensen, T. Lindergaard, U.R. Hansen, G. Mogensen, J. Electrochem. Soc. 141 (1994) 2122.
[15] S. Lubke, H.D. Wiemhofer, Solid State Ionics 117 (1999) 229.
[16] L. Navarro, F. Marques, J. Frade, J. Electrochem. Soc. 144 (1) (1997).
[17] I. Riess, D. Braunshtein, D.S. Tannhauser, J. Am. Ceram. Soc. 64 (1981) 480.
[18] K. El Adham, A. Hammou, Solid State Ionics 9 and 10 (1983) 905.
[19] G.M. Christie, F.O.P.F. van Berkel, Solid State Ionics 83 (1996) 17.
[20] C. Kleinlogel, L.J. Gauckler, Solid State Ionics 135 (2000) 567.
[21] K. Huang, M. Feng, J.B. Goodenough, J. Am. Ceram. Soc. 81 (1998) 357.
[22] G.B. Jung, T.J. Huang, C.L. Chang, J. Solid State Electrochem. 6 (2002) 225–230.
[23] J. Fleigh, J. Maier, J. Electrochem. Soc. 145 (1998) 1781.
[24] J.C.C. Abrantes, J.A. Labrincha, J.R. Frade, J. Eur. Ceram. Soc. 20 (2000) 603.